PCCP

Accepted Manuscript

ROYAL SOCIETY OF CHEMISTRY

www.rsc.org/pccp

Journal Name

RSCPublishing

ARTICLE

Lithium-cyclo-difluoromethane-1,1-bis(sulfonyl)imide as a stabilizing electrolyte additive for improved high voltage application of lithium-ion batteries

aCite this: DOI: 10.1039/x0xx00000x

Received 00th January 2012,
Accepted 00th January 2012

DOI: 10.1039/x0xx00000x

www.rsc.org/

Patrick Murmann[a], Benjamin Streipert[a], Richard Klöpsch[a], Nikolai Ignatiev[b], Peter Sartori[b], Martin Winter[a], Isidora Cekic-Laskovic[a]

Lithium-cyclo-difluoromethane-1,1-bis(sulfonyl)imide (LiDMSI) was evaluated as an electrolyte additive in lithium-ion batteries for improved high voltage application. Cycling the cathode at high potentials leads to an electrochemical oxidation of the salt to form a cathode electrolyte interphase (CEI) layer on the cathode surface. With the addition of 2 wt.% of LiDMSI to the 1 M $LiPF_6$ in EC:DEC 1:1 (by wt.) electrolyte, the capacity retention and the Coulombic efficiency in $LiNi_{1/3}Co_{1/3}Mn_{1/3}O_2$ / Li-half-cells as well as $LiNi_{1/3}Co_{1/3}Mn_{1/3}O_2$ / graphite-full-cells was improved. The cycling results point at less over-potential and resistance at the cathode/electrolyte interface. These improvements are studied by SEM, EIS as well as XPS techniques.

Introduction

One of the crucial challenges for the further development of lithium ion batteries (LIBs) is to gather alternatives to the state-of-the-art-materials in order to enhance the energy density. [1]
By now, there are promising alternatives to replace graphite as anode material with materials having higher capacities. [2] For instance, silicon depicts a theoretical capacity up to 10 times higher than graphite. [3, 4] However, for LIB cathode materials, a comparable increase seems impracticable in the next years. Still today, the bottleneck for an increase in specific energies (Wh/kg) is the low specific charge (Ah/kg) of the cathode material. [5] However, recent activities in research and development on cathode materials are leading in the direction of so called high voltage cathodes, that are charged beyond the typical potentials of 4.2 – 4.3 V vs. Li/Li^+ and thus also display a discharge at higher potentials than usual. [6] The high-voltage (HV) cathode materials with layered structure also display a higher discharge capacity, when charged to higher potentials. A well-known example is the layered $LiNi_{1/3}Co_{1/3}Mn_{1/3}O_2$ (NCM). Compared to $LiCoO_2$, NCM is thermally and electrochemically more stable at higher potentials and the presence of Mn^{4+} in the lattice suppresses the undesired structural changes of this material. For this reason, higher anodic cut-off potentials (e.g. 4.6 V vs. Li/Li^+) and larger specific capacities can be attained. [7-10]

The increase in capacity as well as in working potential leads to a quadratic increase in specific energy. [11] However, charging to such high potential values can lead to a significant decrease in cycle life. [9, 10, 12] The high working potential does not only provoke structural changes of the NCM material [11, 13, 14], but also induces electrolyte decomposition at the cathode/electrolyte interface, since a potential of 4.6 V vs. Li/Li^+ is beyond the stability range of the organic carbonate electrolyte solvents, in most cases a mix of cyclic (ethylene carbonate (EC)) and linear carbonates (diethyl carbonate (DEC), dimethyl carbonate (DMC) and ethyl methyl carbonate (EMC)). [14-18] There have been numerous approaches in order to overcome the electrolyte instability at the cathode/electrolyte interface; for example, the addition of an electrolyte additive that decomposes and forms a protective cathode electrolyte interphase (CEI) layer on the cathode surface and thus suppresses further decomposition of the electrolyte at the electrode. [12, 19-21] Possible CEI film forming additives are required to display an anodic stability that lies below that of the base electrolyte. Then, the additive can decompose on the

surface and form a CEI layer before the main electrolyte components would be affected by the oxidation potential. A wide variety of electrolyte additives have been discussed in literature so far; among them vinylene carbonate (VC), which shows positive influence on both the anode and the cathode side. [22-27] Moreover, electrolyte salts such as lithium bis(oxalato)borate (LiBOB) [28] or lithium difluoro-(oxalato)borate (LiDFOB) [29, 30] have been utilized as film forming additives at the cathode, taking additional advantage of the fact, that they also improve the performance of the solid electrolyte interphase (SEI) on graphite. [31]

In this work, the salt lithium-cyclo-difluoromethane-1,1-bis(sulfonyl)imide (LiDMSI), was investigated as a film forming additive as its anodic stability of about 4.3 V vs. Li/Li^+ is known to be lower than the components used in the reference electrolyte (1 M $LiPF_6$ in EC:DEC 1:1, by wt.). [32, 33] This work aims towards the investigation of the CEI layer and its influence on the cycling behaviour of NCM. The results are compared to the results obtained for the reference electrolyte without the electrolyte additive.

Experimental

Electrode preparation

Positive electrodes for the constant current cycling as well as for the analytical and spectroscopic experiments consisted of $LiNi_{1/3}Co_{1/3}Mn_{1/3}O_2$ (NCM, Toda) as active material. The slurry of the cathode electrodes contained 85 wt.% NCM, 8 wt.% Super C65 (Imerys) and 7 wt.% Polyvinylidene difluoride (PVdF Kynar 761, Arkema) with N-methyl pyrrolidone (NMP, Fluka Inc.) and was coated on an aluminium foil current collector. The active mass loading of the electrodes was approximately 5 mg cm^{-2}.

The negative electrodes consisted of T44 graphite (Imerys) and the slurry for the electrodes was composed of 87 wt.% T44 graphite, 5 wt.% Super C65 (Imerys) and 8 wt.% Polyvinylidene difluoride (PVdF Kynar 761, Arkema) dissolved in dimethylformamide (DMF, Sigma Aldrich) and coated on a copper foil current collector. The active mass loading of the electrodes was approximately 2.2 mg cm^{-2}.

Electrolyte preparation and cell assembly

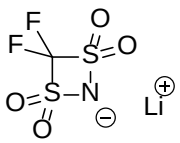

Scheme 1: Structural formula of lithium-cyclo-difluoromethane-1,1-bis(sulfonyl)imide (LiDMSI).

A solution of 1 M $LiPF_6$ (BASF, battery grade) in EC:DEC 1:1, by wt. (BASF, battery grade) was used as reference electrolyte. The investigated salt LiDMSI was dried under reduced pressure at 60 °C before use. For the second electrolyte solution 2 wt.% of LiDMSI was added to the reference electrolyte. Both electrolyte mixtures were prepared in a glove box under argon atmosphere (MBraun, H_2O and O_2 < 0.1 ppm).

A three electrode Swagelok® cells setup was used for both the constant current cycling test and the electrochemical conditioning of the electrode samples for the analytical investigations.

Half-cell constant current cycling tests were performed with lithium foil as counter (CE, 12 mm ∅) and reference electrode (RE, 5 mm ∅) while the working electrode (WE, 12 mm ∅) consisted of the NCM-based composite. Whatman GfD fleece was used as separator. Sufficient cells were cycled with both electrolytes in order to eliminate statistical errors and provide enough material for the analysis of the cycled electrodes.

Electrochemical impedance measurements were performed after cycling with the same setup as described above.

Full cell constant current cycling tests were performed with NCM as WE, T44 graphite as CE and lithium as RE. While the NCM electrode showed a capacity of 0.6 - 0.7 mAh and a specific current for 1C of 140 mA g^{-1}, the specific current of the graphite was set to 360 mA g^{-1}. The mass balance in the full cells was fixed to a 15% higher capacity for the anode.

Electrochemical measurements

The conductivity measurements were performed with custom-made cells containing a two stainless steel electrode arrangement with a diameter of 4 mm for each electrode. For the conductivity measurements a Solartron 1260A impedance gain phase analyzer was used in combination with a Solartron 1287A potentiostat. By setting the polarization parameters to 0 V vs. open circuit for the DC potential, an AC amplitude of 20 mV was applied. A frequency sweep was set from the initial frequency of 1 MHz to 10 kHz (logarithmic).

Electrochemical investigations were performed at 20 °C (± 2 °C) using a MACCOR Series 4000 battery tester. The NCM/Li half-cell cycling experiment test plan consisted of three cycles functioning as formation cycles with a C-rate of C/5, followed by 47 cycles with a C-rate of 1C for the charge and discharge steps, respectively. The potential ranged from 3.0 V to 4.6 V vs. Li/Li^+ for the insertion and de-insertion steps, respectively.

The full-cell cycling test plan consisted of 5 formation cycles at C/10 for charge and discharge. Afterwards, the cells were cycled at 1C in a cell voltage range of 2.8 V to 4.5 V. The delithiation step (charge) of the cathode was supported by an additional constant voltage charging step at the end-of-charge voltage (EOC), until the current rate went below C/5. For the lithiation step (discharge), a constant current rate of 1C was applied. In order to monitor the individual potential values of the two electrodes separately, a three electrode arrangement with lithium as RE, was chosen.

AC electrochemical impedance spectroscopy (EIS) was performed after the 3rd and the 50th cycle at the open circuit potential (OCP) at a frequency range between 1 mHz and 1

MHz with a sinus amplitude of 5 mV using a Solartron 1260 A impedance gain phase analyzer.

Analytical measurements

Scanning electron microscopy (SEM) was performed on pristine and cycled electrodes (50th cycles) on a Zeiss Auriga® CrossBeam workstation with an acceleration voltage of 3 kV.
For X-ray photoelectron spectroscopy (XPS) measurements, pristine and cycled electrodes were used. In order to examine the CEI layer, electrodes were investigated after three and after fifty cycles with the reference electrolyte as well as the additive containing electrolyte. The cells were disassembled under protective atmosphere without washing the electrodes due to the unknown solubility of the CEI layer compounds in certain washing solutions. [34-36] Afterwards, the electrodes were transported in a sealed container to the glovebox connected to the XPS to suppress any exposure to the atmosphere. The XPS measurements (Axis Ultra DLD, Kratos) were carried out at a 0° angle of emission and a pass energy of 20 eV using a monochromatic Al Kα source (hν = 1486.6 eV) at a 10 mA filament current and a 12 kV filament voltage source energy. In order to compensate the charging of the sample, a charge neutralizer was used. The analysis area was approximately 300 × 700 µm. For reproducibility reasons, two electrodes of each electrolyte after the aforementioned cycle number were measured and on each of the electrodes three points were measured and arithmetically averaged.

Results and discussions

Half-cell constant current experiments on NCM electrodes were conducted at 4.6 V vs. Li/Li$^+$ (Figure 1). The discharge (=insertion capacities) and the Coulombic efficiencies are plotted versus the cycle number, whereby the performance of the electrolyte with 2 wt% LiDMSI is compared to the reference electrolyte (1 M $LiPF_6$ in EC:DEC 1:1, by wt.). Within the initial three formation cycles (C/5), both cells show comparable capacities of approximately 190 mAh g^{-1}, although the capacities obtained with the additive containing electrolyte are slightly higher. However, under faster cycling conditions (1C) the reference electrolyte displays a capacity fading of the insertion capacity from 167 mAh g^{-1} to 144 mAh g^{-1} compared to the LiDMSI containing electrolyte with a capacity fading only from 172 mAh g^{-1} in the 4th cycle to 164 mAh g^{-1} in the 50th cycle. This results in capacity retention of 86% for the cell with the reference electrolyte and 96% for the cell with the electrolyte additive over 47 cycles. Not only the distinct superior capacity retention, but also the Coulombic efficiency displays higher and increasing values over 50 cycles for the LiDMSI containing electrolyte, while the efficiency of the reference electrolyte stays constant at a lower value (Figure 1). With these higher capacities at 1C for the additive containing electrolyte an increased performance not only in capacity retention but also in rate behaviour is notable.

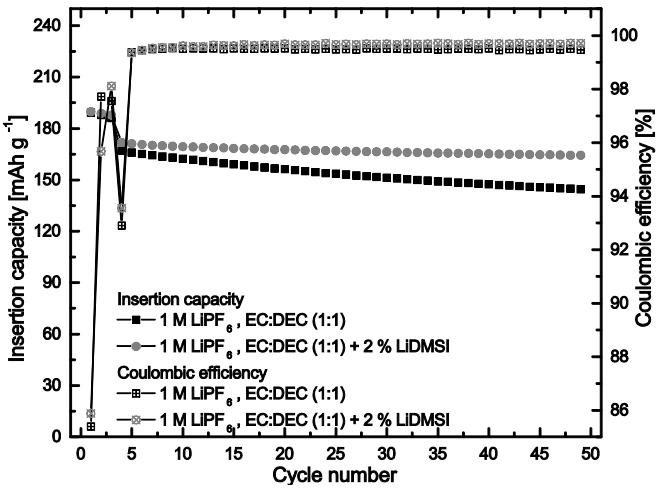

Figure 1: Constant current cycling of the reference electrolyte (1 M $LiPF_6$ in EC:DEC 1:1, by wt.) and the LiDMSI containing electrolyte at 20°C over 50 cycles . The rates of the first three cycles were C/5 and for the following 47 cycles 1C. The potential range is 3 V to 4.6 V vs. Li/Li$^+$. Both, the insertion capacity (=discharge capacity) and the Coulombic efficiency are plotted versus the cycle number.

To shed light on the origin of capacity fading, the potential vs. capacity plots of both electrolytes for the 3rd and the 50th cycle of the constant current half-cell cycling experiment are presented in Figure 2. In line with the cycling behavior (Figure 1), both potential profiles overlap almost perfectly in the 3rd cycle, but show pronounced differences in the 50th cycle. Compared to the reference electrolyte, NCM cycled with the LiDMSI containing electrolyte exhibits a lower over-potential for the charge and the discharge step.
Due to the higher over-potentials of NCM in the reference electrolyte of ca. 150 mV (Figure 2a, vertical arrows), the cut-off criteria of 4.6 V vs. Li/Li$^+$ and 3.0 V vs. Li/Li$^+$ for charge and discharge, respectively, are reached earlier. Therefore, less lithium de-insertion (= charge) and insertion (= discharge) takes place and results in lower capacities of NCM in the reference electrolyte compared to the LiDMSI containing one. This phenomenon is indicated by horizontal arrows in Figure 2a. Taking into account that the presence of LiDMSI showed no influence on the ionic conductivity of the electrolyte and that the electrodes were of the same weight, the over-potential is assumed to result from a CEI layer on the cathode that is hindering electrode kinetics.

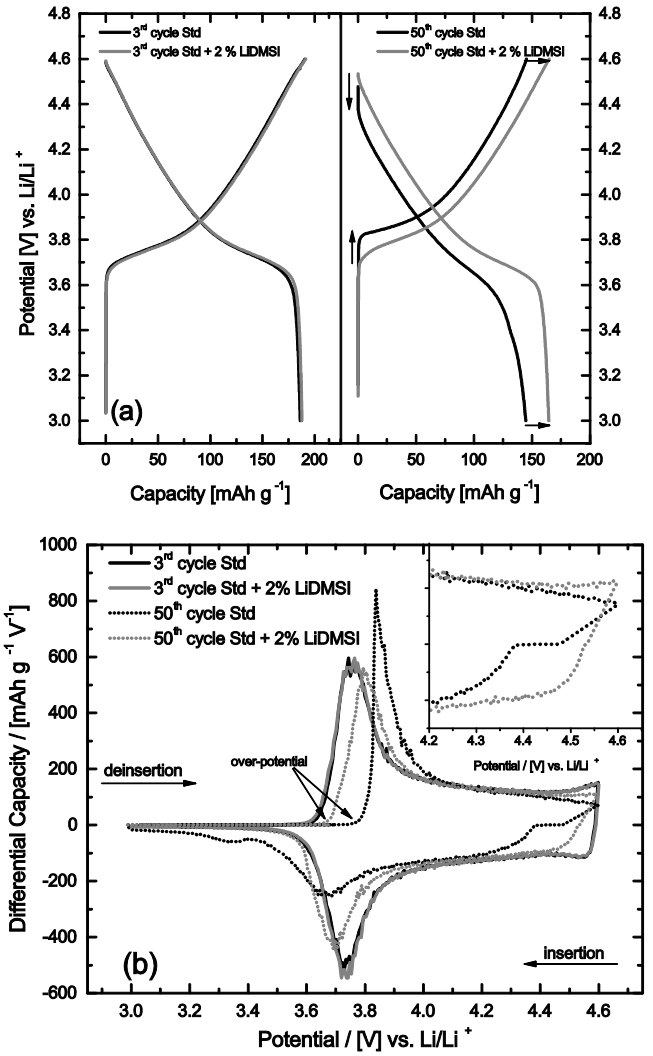

Figure 2: (a) 3rd and 50th cycle of the constant current cycling experiment of NCM depicted as a potential vs. capacity plot of the reference electrolyte (1 M $LiPF_6$ in EC:DEC 1:1, by wt.) and the LiDMSI containing electrolyte 20°C in the potential range from 3 to 4.6 V vs. vs. Li/Li^+. The rates of the third cycles were C/5 and for the 50th cycle 1C. (b) Corresponding differential capacity (dQ/dV) plots of the 3rd and 50th cycle. The insert shows an enlargement of the response to the high potential region of the 50th cycle.

The differential capacity plots of the 3rd and the 50th cycle (Figure 2b) confirm this interpretation of the over-potentials. Once again, the curves of the 3rd cycle obtained in both investigated electrolytes overlap almost perfectly, while in the 50th cycle clear differences are noticeable.

First of all, the difference in the charge curves in the 50th cycle is distinct. The over-potential of the cells after the 50th cycle compared to the 3rd cycle is clearly visible. The de-insertion peak of the 3rd cycle starts at a potential of 3.6 V vs. Li/Li^+ and the shift due to over-potentials in the 50th cycle is only 50 mV for the additive containing electrolyte , but 150 mV for the reference electrolyte. Obviously, the over-potential correlates to a distinguishable shift of the insertion and de-insertion potentials and, therefore, to an earlier termination of the charge and discharge steps. As the over-potential of NCM is lower in the case of the LiDMSI containing electrolyte, the capacity fading is less intense and higher capacities are reached after several cycles compared to the reference electrolyte. An additional reason for the higher over-potential is the increased C-rate from C/5 in the 3rd cycle (last formation cycle) to the 1C in the following cycles.

Another difference in the curves of the 3rd and the 50th cycle can be observed at higher cathode potentials. Since NCM exhibits a sloping potential profile, it can attain more charge capacity when increasing the cut-off potential (insert in Figure 2b for the 50th cycle). [37] Correspondingly, the differential capacity does not drop down to 0 mAh $g^{-1}V^{-1}$ and even increases towards the cut-off potential of 4.6 V vs. Li/Li^+ for the 3rd cycle. While the curves in the 3rd and 50th cycle of the LiDMSI additive containing cell vary only marginally, the reference electrolyte cell shows a constant decrease of the differential capacity when approaching the cut-off potential and displays a drop of more than 200 mV directly afterwards.

Based on the above described promising performance on NCM and on our previous report [32], showing that LiDMSI has no detrimental effect on the performance of graphitic anodes, we evaluated full NCM / graphite cells at higher cell voltages. To prevent any lithium plating on the anode surface, the anode capacity exceeded that of the cathode by 15 %. To approach the cut-off potentials in the half-cells measured vs. lithium metal reference, a cell cut-off voltage from 2.8 V to 4.5 V vs. Li/Li^+ was applied. Figure 3 shows the specific capacity (with regard to the electrode, which is limiting the cell capacity, i.e. the cathode) and the fading rate plotted versus the cycle number of the reference electrolyte and the LiDMSI containing electrolyte. Starting with roughly the same specific capacity in the first cycle, a decrease is observable within the five formation cycles (C-rate: C/10). However, the fading of the reference electrolyte is steeper than for the LiDMSI containing electrolyte.

Starting at the 6th cycle with a C-rate of 1C, the cell with the LiDMSI containing electrolyte cycles at about 140 mAh g^{-1}, while the capacity of the cell with the reference electrolyte shows a capacity of 130 mAh g^{-1}. In addition, the capacity fading is displayed in Figure 3 for both electrolyte systems. The reference electrolyte displays a higher fading rate of 81 % compared to 87 % for the LiDMSI containing electrolyte. The Coulombic efficiency does not show reasonable differences at approximately 99.5 %. The fact that the additive improves the cycling of the NCM not only in half-cells but also in full-cells as well as the reported electrochemical decomposition of the LiDMSI starting closely after 4.3 V vs. Li/Li^+ indicate, that the influence of the additive derives from the cathode and not from the lithium counter electrode. [32]

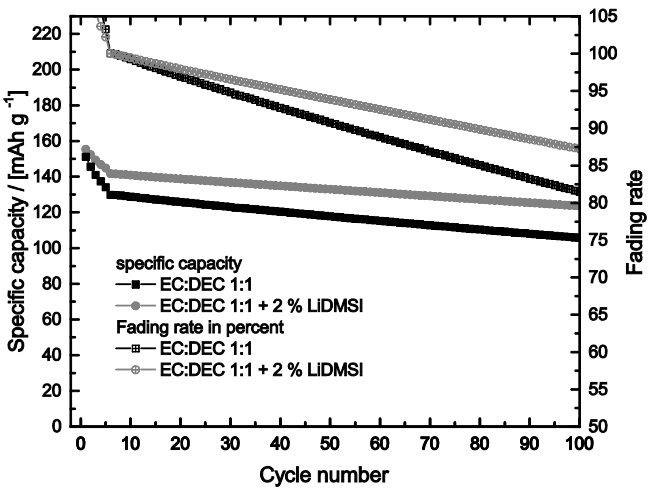

Figure 3: Constant current cycling of graphite T44/NCM full-cells of the two investigated electrolytes over 100 cycles at 20°C. The cells were cycled in a voltage range from 2.8 V to 4.5 V vs. Li/Li$^+$ with five formation cycles at C/10 followed by 95 cycles at 1C. The specific capacity and the fading rate are plotted versus the number of cycles.

SEM was conducted in order to image the CEI layer on NCM formed during cycling. Figure 4 displays magnifications of the pristine, uncycled NCM electrode at the top, the electrode with the LiDMSI containing electrolyte after 50 cycles in the middle and the electrode with the reference electrolyte after 50 cycles at the bottom. The respective inserts show the whole NCM particle for each sample.

The surface of the pristine NCM electrode is relatively homogeneous without a surface layer. The other two samples, imaged after 50 cycles in electrolytes with and without addition of LiDMSI show signs of a surface layer. The surface of the electrode cycled with the LiDMSI containing electrolyte depicts a quite uniform layer which covers each particle. At the surface of the electrode cycled in the reference electrolyte, localized areas of decomposition products are visible, however not as a uniform layer. These spots are common for carbonate based electrolytes that utilize $LiPF_6$ as conductive salt and are not of further interest since no uniform layer is observable. Judging from the SEM images, it seems that the electrode cycling in the presence of LiDMSI formed a uniform surface layer, in contrary to the reference electrolyte.

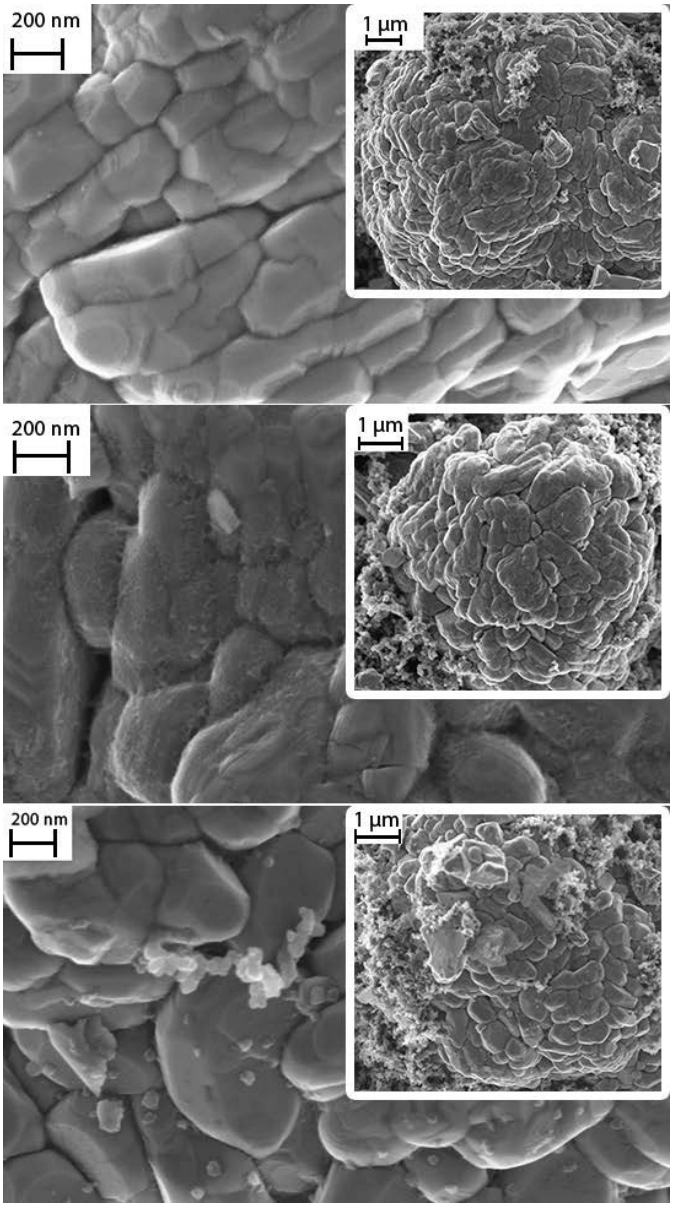

Figure 4: SEM images of NCM electrodes (top) pristine electrode, (middle) after 50 cycles with the LiDMSI containing electrolyte and (bottom) after 50 cycles with the reference electrolyte. The insert shows a whole NCM particle of the respective electrode.

To further investigate the effect of the CEI layers, electrochemical impedance spectroscopy (EIS) was performed after the 3rd and the 50th cycle, respectively, using the NCM / Li half-cell setup. Having in mind that the impedance depends on the state-of-charge (SOC) and in order to be able to compare the data, the measurements were performed in the discharged state. The impedance data is interpreted according to previous reports of on additives in high voltage cathode material cells. [12, 38] The semicircle appearing in the high frequency range can be attributed to the Li$^+$ ion migration resistance through the surface of the cathode (R_f), while the semicircle in the range of medium-to-low frequencies can be interpreted as the charge transfer resistance between the electrolyte and the electrode

(R_{ct}). The tail end in the low frequency range is due to Li^+ diffusion in the solid particles of the electrode.

Figure 5 displays the behavior of the half-cells, the straight lines depict the 3rd cycle and the dashed line the 50th cycle. It is observable that for the reference electrolyte, the R_f value is distinctively smaller than for the electrolyte with LiDMSI after the 3rd cycle. However, after the 50th cycle, R_f is increased for the reference electrolyte, while for the electrolyte with LiDMSI the impedance even slightly decreases. These results indicate that in the case of cycling with the reference electrolyte, the CEI layer grows with cycle number, which can be explained by the fact that the formed CEI is not protective against further decomposition. However, in case of the additive containing electrolyte, the CEI layer after the 3rd cycle does not grow within the 50 cycles and stays stable in size, indicating that in the presence of LiDMSI a protective CEI is formed. Besides R_f, in case of the LiDMSI containing electrolyte, also R_{ct} stays almost at the same level, which is in line with our interpretation that the CEI layer does not grow during cycling. As a result, electrolyte decomposition and / or electrode deterioration is suppressed and better cycling behavior and higher capacity retention is achieved (Figures 1 and 3).

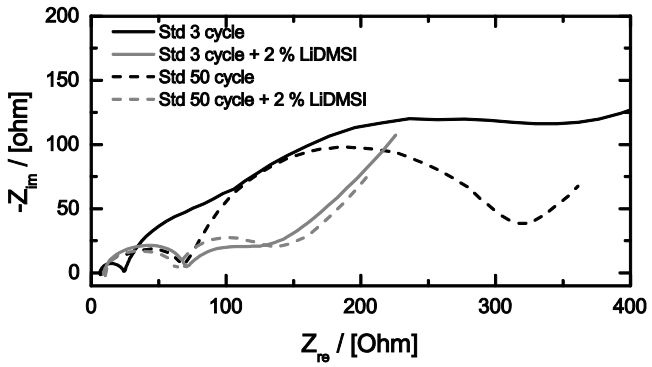

Figure 5: AC impedance spectra of NCM / Li half-cells in the discharged state after the 3rd (straight line) and 50th (dashed line) cycle, respectively, cycled with the two investigated electrolytes.

Niehoff et al. determined the thickness of the surface layer on different anode and cathode materials, including NCM, via X-ray photoelectron spectroscopy (XPS). [34-36]

To underline the results of the EIS spectra, i.e. that the CEI layer is not growing with cycling due to the presence of LiDMSI in the electrolyte, XPS measurements were conducted to calculate the thickness of the CEI layer of the particular electrodes.

The thickness d_{diff} of the CEI layer can be estimated by equation 1.

$$d_{\mathrm{diff}} = ln\frac{I_a}{I_b} * \lambda_{ads}\cos(\theta_e)\, t_{factor} \qquad \text{(equation 1)}$$

Here, I_a amounts to the thickness of the NCM substrate (in $\%_{at}$) without any CEI layer on top. I_b depicts the thickness of the substrate value at the current cycled condition. The mean free path of the total decomposition layer λ_{ads} at the binding energy of Mn 2p in the NCM signal was calculated by using the TPP (Tanuma, Powell, Penn) equations and amounts to 20.52 Å. [39, 40] The angle of emission is displayed by $\theta = 0°$ and the topographic factor (t_{factor}) is set to 0.67, which is taking the topography of the sample as a sphere into account.

Table 1 displays the layer thickness of electrodes cycled with and without the LiDMSI in the electrolyte. The values amount to the average of two measured electrodes and the mean deviation is given in the third column.

Table 1: CEI layer thickness on top of the NCM electrode after the 3rd and the 50th cycle for the reference electrolyte and the LiDMSI containing electrolyte, respectively

	Layer thickness [Å]	Mean deviation
Reference electrolyte after 3rd cycle	13	2.20
Reference electrolyte after 50th cycle	17	0.17
LiDMSI containing electrolyte after 3rd cycle	11	5.50
LiDMSI containing electrolyte after 50th cycle	10	0.72

After the 3rd cycle, the deviation of the CEI layer thickness is high for both electrolyte formulations, indicating an unfinished formation state of the layers. This suggests that the three formation cycles are not sufficient to form a uniform and reproducible CEI layer on the NCM electrodes. Further, by repeating the measurements after the 3 cycles, similar results were obtained. However, after the 50th cycle, the deviation for both electrolyte solutions becomes low, indicating that the CEI layer formation is more complete.

The thickness of the LiDMSI containing electrolyte stays almost constant after the 3rd and 50th cycle at approximately 10.5 Å, which is in line with the EIS results showing almost constant impedance during cycling. For the reference electrolyte, the EIS measurements showed that the R_f of the CEI layer after the 3rd cycle was lower than after the 50th cycle and even lower than for the measurements with the LiDMSI containing electrolyte after the 3rd and 50th cycle, respectively. As the impedance measurement takes the resistivity into account, the layer thickness does not have to correlate to that directly. For the reference electrolyte, the thickness after the 3rd cycle is 13 Å and increases to almost 17 Å after the 50th cycle. The layer obtained in the reference electrolyte is thicker than the layer obtained in the additive containing electrolyte, although R_f is smaller after the 3rd cycle. The XPS as well as the EIS data point out that the CEI layer formed on NCM in the LiDMSI containing electrolyte is stable over 50 cycles.

Conclusions

LiDMSI is proposed and investigated as an electrolyte additive to improve the capacity retention and the Coulombic efficiency of NCM in half-cells and NCM / graphite full-cells cycled at the elevated potential of 4.6 V vs. Li/Li^+. In NCM / Li half-cells, the capacity retention after 50 cycles was improved heavily by the additive. Reasonable explanation lies in lower over-potentials. SEM images showed the existence of a CEI layer which was further investigated by EIS and XPS to determine a constant impedance during cycling and an almost constant thickness of the CEI layer. It can be concluded that LiDMSI is suitable for applications as electrolyte additive for high-voltage lithium ion batteries with NCM and other high voltage cathodes.

Acknowledgements

The work was supported by the German Research Foundation Project (DFG) WI 2929/6-1 and through the project Electrolyte Lab (4E) – 29120340 (BMBF).

Notes and references

[a]: Westfälische Wilhelms-Universität Münster, Institute of Physical Chemistry, MEET Battery Research Center, Corrensstr. 46, 48149 Muenster, Germany

[b]: Universität Duisburg-Essen former Universität Duisburg, Institute of Instrumental Analytic, 45141 Essen, Germany

1. R. Wagner, N. Preschitschek, S. Passerini, J. Leker and M. Winter, *J Appl Electrochem*, 2013, **43**, 481-496.
2. U. Kasavajjula, C. S. Wang and A. J. Appleby, *J Power Sources*, 2007, **163**, 1003-1039.
3. M. N. Obrovac and L. J. Krause, *J Electrochem Soc*, 2007, **154**, A103-A108.
4. W. R. Liu, N. L. Wu, D. T. Shieh, H. C. Wu, M. H. Yang, C. Korepp, J. O. Besenhard and M. Winter, *J Electrochem Soc*, 2007, **154**, A97-A102.
5. A. Kraytsberg, Y. Kraytsberg, A. Ein Eli and Kraytsberg, *Adv Energy Mater*, 2012, **2**, 922-939.
6. M. Hu, X. L. Pang and Z. Zhou, *J Power Sources*, 2013, **237**, 229-242.
7. P. He, H. J. Yu, D. Li and H. S. Zhou, *J Mater Chem*, 2012, **22**, 3680-3695.
8. B. J. Hwang, Y. W. Tsai, D. Carlier and G. Ceder, *Chem Mater*, 2003, **15**, 3676-3682.
9. Y. K. Sun, S. W. Cho, S. W. Lee, C. S. Yoon and K. Amine, *J Electrochem Soc*, 2007, **154**, A168-A172.
10. K. M. Shaju, G. V. S. Rao and B. V. R. Chowdari, *Electrochim Acta*, 2002, **48**, 145-151.
11. H. H. Zheng, Q. N. Sun, G. Liu, X. Y. Song and V. S. Battaglia, *J Power Sources*, 2012, **207**, 134-140.
12. Y.-S. Lee, *J Power Sources*, 2011, **196**, 6997.
13. F. La Mantia, F. Rosciano, N. Tran and P. Novak, *J Appl Electrochem*, 2008, **38**, 893-896.
14. S. S. Zhang, *J Power Sources*, 2006, **162**, 1379-1394.
15. R. Marom, S. F. Amalraj, N. Leifer, D. Jacob and D. Aurbach, *J Mater Chem*, 2011, **21**, 9938-9954.
16. J. M. Tarascon and D. Guyomard, *Solid State Ionics*, 1994, **69**, 293-305.
17. K. C. Moller, T. Hodal, W. K. Appel, M. Winter and J. O. Besenhard, *J Power Sources*, 2001, **97-98**, 595-597.
18. M. Winter, R. Imhof, F. Joho and P. Novak, *J Power Sources*, 1999, **81**, 818-823.
19. A. von Cresce, *J Electrochem Soc*, 2011, **158**, A337.
20. A. von Cresce and C. von, *ECS Transactions*, 2012, **41**, 17.
21. S. Ahn, H. S. Kim, S. Yang, J. Y. Do, B. H. Kim and K. Kim, *J Electroceram*, 2009, **23**, 289-294.
22. D. Aurbach, K. Gamolsky, B. Markovsky, Y. Gofer, M. Schmidt and U. Heider, *Electrochim Acta*, 2002, **47**, 1423-1439.
23. D. Aurbach, B. Markovsky, A. Rodkin, E. Levi, Y. S. Cohen, H. J. Kim and M. Schmidt, *Electrochim Acta*, 2002, **47**, 4291-4306.
24. K. Abe, K. Miyoshi, T. Hattori, Y. Ushigoe and H. Yoshitake, *J Power Sources*, 2008, **184**, 449-455.
25. K. C. Moller, H. J. Santner, W. Kern, S. Yamaguchi, J. O. Besenhard and M. Winter, *J Power Sources*, 2003, **119**, 561-566.
26. C. Korepp, H. J. Santner, T. Fujii, M. Ue, J. O. Besenhard, K. C. Möller and M. Winter, *J Power Sources*, 2006, **158**, 578-582.
27. H. J. Santner, C. Korepp, M. Winter, J. O. Besenhard and K. C. Moller, *Anal Bioanal Chem*, 2004, **379**, 266-271.
28. S. Y. Ha, J. G. Han, Y. M. Song, M. J. Chun, S. I. Han, W. C. Shin and N. S. Choi, *Electrochim Acta*, 2013, **104**, 170-177.
29. Y. Zhu, Y. Li, M. Bettge and D. P. Abraham, *J Electrochem Soc*, 2012, **159**, A2109-A2117.
30. S. Zugmann, M. Fleischmann, M. Amereller, R. M. Gschwind, M. Winter and H. J. Gores, *J Chem Eng Data*, 2011, **56**, 4786-4789.
31. M. Winter, *Zeitschrift für physikalische Chemie*, 2009, **223**, 1395.
32. P. Murmann, P. Niehoff, R. Schmitz, S. Nowak, H. Gores, N. Ignatiev, P. Sartori, M. Winter and R. Schmitz, *Electrochim Acta*, 2013, **114**, 658-666.
33. P. Sartori, N. Ignat'ev, C. Junger, R. Juschke and P. Rieland, *J Solid State Electr*, 1998, **2**, 110-116.
34. P. Niehoff and M. Winter, *Langmuir*, 2013, **29**, 15813-15821.
35. P. Niehoff, S. Passerini and M. Winter, *Langmuir*, 2013, **29**, 5806-5816.
36. P. Niehoff, E. Kraemer and M. Winter, *J Electroanal Chem*, 2013, **707**, 110-116.
37. J. T. Son and E. J. Cairns, *Electrochem Solid St*, 2006, **9**, A27-A30.
38. S. Tan, Z. R. Zhang, Y. X. Li, Y. Li, J. M. Zheng, Z. B. Zhou and Y. Yang, *J Electrochem Soc*, 2013, **160**, A285-A292.
39. S. Tanuma, C. J. Powell and D. R. Penn, *Surf Interface Anal*, 2003, **35**, 268-275.
40. S. Tanuma, C. J. Powell and D. R. Penn, *Surf Interface Anal*, 1994, **21**, 165-176.